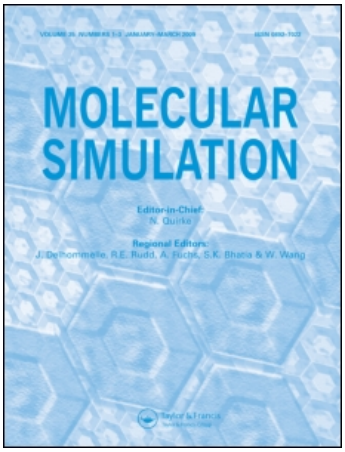

Molecular Simulation
Publication details, including instructions for authors and subscription information:
http://www.informaworld.com/smpp/title~content=t713644482

A molecular dynamics simulation of hexagonal solid platinum nanowires

Q. H. Cheng[a]; C. Lu[a]; H. P. Lee[a]
[a] Institute of High Performance Computing, Singapore, Singapore

To cite this Article Cheng, Q. H. , Lu, C. and Lee, H. P.(2005) 'A molecular dynamics simulation of hexagonal solid platinum nanowires', Molecular Simulation, 31: 4, 289 — 293
To link to this Article: DOI: 10.1080/08927020412331333720
URL: http://dx.doi.org/10.1080/08927020412331333720

Molecular Simulation, Vol. 31, No. 4, 15 April 2005, pp. 289–293

Taylor & Francis
Taylor & Francis Group

A molecular dynamics simulation of hexagonal solid platinum nanowires

Q.H. CHENG*, C. LU and H.P. LEE

Institute of High Performance Computing, 1 Science Park Road, #01-01 The Capricorn, Singapore 117528, Singapore

(Received May 2004; In final form June 2004)

Experimental evidence of the existence of multi-wall platinum (Pt) nanowires (NWs) has been reported. In this paper, we investigated structural formation of Pt NWs using the classical molecular dynamics (MD) simulation method. The simulations began from initial configurations with random distributions of atomic positions. The initial configuration was minimised by the steepest descent method, and assigned a temperature of 601 K with a random distribution of atomic velocities. Then simulated annealing was applied such that the temperature of the system was reduced gradually to 1 K and a stable NW structure was obtained. Types of hexagonal solid Pt NWs featuring different structures than those of previously reported NWs were found. Details of structural characteristics and mechanical properties of these Pt NWs are presented.

Keywords: Nanowire; Molecular dynamics simulation; Steepest descent method; Periodic boundary condition; Velocity Verlet algorithm; Berendsen thermostat

1. Introduction

Nanowire (NW) is an important candidate component of nanoelectronic devices. Formation and structural properties of thin metallic NW have been extensively studied in the past decade. Interest has been paid to several fcc metals such as Au, Cu and Al, and various structural forms have been experimentally and analytically found. Kondo and Takayanagi [1] reported fabrication of helical multi-shell (HMS) Au NWs. Bilalbegovic [2,3] observed by molecular dynamics (MD) simulation the existence of multi-shelled and filled metallic NWs depending on the metal and initial configuration. He also examined the stability and melting properties of Au NW [4,5]. Kang and Hwang [6–10] simulated ultrathin Cu NWs of rectangular and pentagonal types and several cylindrical multi-shell (CMS) types. Hasmy [11] described MD simulations with embedded atom potentials to compute the properties of Au NW and nanofilms that are of interest for the development of future nanoelectronic devices.

Platinum (Pt) NWs were much less studied than Au and Cu NWs. Pt NWs have been fabricated by several investigators using various reported methods. Oshima *et al.* [12] used an electron-beam irradiation technique to fabricate a Pt NW *in situ* in an ultrahigh vacuum transmission electron microscope (UHV-TEM). They presented experimental evidence that the Pt NW was of a HMS structure. Arrays of Pt NWs were fabricated by electro-depositing Pt metal into nanoporous anodic aluminium oxide (AAO) templates [13]. This technique was also employed by Kong *et al.* [14]. Rodrigues and Ugarte [15] studied atomic arrangement and electrical transport properties of Au and Pt NWs generated by mechanical elongation using *in situ* high-resolution transmission electron microscopy (HRTEM). Theoretical works on Pt NWs were scarce. Finbow *et al.* [16] conducted MD simulations to investigate stretching and failure mechanism of Pt and Ag NWs. However, studies on structural configuration of Pt NWs by simulation were not found.

In this paper, MD simulations of Pt NWs have been carried out. The motivation is to investigate the atomic structural characteristics of Pt NWs, which are formed in MD simulation similar to a self-organisation process. The previously reported HMS and CMS NWs consisted of walls formed by rolling a fcc (1 1 1) triangular network sheet [2–10]. However, no details of NW structures were provided in those papers. In our investigations, we obtained Pt NWs consisting of different structural forms as described in this paper. In future study, we would investigate the reason that caused differences in structure formation of metallic NWs.

*Corresponding author. E-mail: chengqh@ihpc.a-star.edu.sg

Molecular Simulation
ISSN 0892-7022 print/ISSN 1029-0435 online © 2005 Taylor & Francis Group Ltd
http://www.tandf.co.uk/journals
DOI: 10.1080/08927020412331333720

2. Sutton–Chen potential

In this work, we investigated structural formation of thin and ultra-thin Pt NWs using a classical MD simulation. Interactions between Pt atoms were described by the Sutton–Chen many body potential [17], which has the form of the potential first proposed by Finnis and Sinclair [18] consisting of a repulsive pairwise term and a bonding term proportional to the square root of a local density representing the cohesive energy of the electrons. The two potentials differ in the way in which the repulsion and the local density are expressed. In the Finnis–Sinclair potential, a parabolic form was adopted for the cohesive energy and a quartic polynomial for the pair repulsion energy. Sutton and Chen [17] added to conventional pair-potential with a term which effectively combines a *N*-body potential for description of short-range interactions and reasonable description of surface relaxation, with a van der Waals tail for a correct description of the long-range interactions. The total potential energy of an atomic system is written as

$$V = \varepsilon \left[\sum_{i>j} \left(a_0/r_{ij}\right)^n - c \sum_i \rho_i^{1/2} \right] \tag{1}$$

where a_0 is the lattice parameter, r_{ij} is the distance between atoms i and j and ρ_i represents local particle density, given by

$$\rho_i = \sum_{i>j} \left(a/r_{ij}\right)^m \tag{2}$$

The exponents determine the range and shape of the potential and the parameters ε and a_0 determine the scales of energy and length, respectively. Requiring n and m are integers and that $n > m > 6$ for each metal in Sutton and Chen [17], m and n were estimated and truncated using the condition that the product mn is proportional to the ratio of bulk modulus to the cohesive energy per unit volume. The experimental cohesive energy and crystal lattice parameter were fitted exactly, and the bulk modulus was fitted within a few per cent of the experimental value, though not exactly. The ratio of the shear to the bulk modulus depends on the difference of the exponents, i.e. $n - m$. After m and n were obtained, ε was then calculated from the cohesive energy and c from an equilibrium condition. For different metals, same values of m and n may be found. In this case, results obtained for one metal may be directly converted into results for the other simply by rescaling the units of energy and length. The constants for Pt taken from Sutton and Chen [17] are $\varepsilon = 19.83\,\text{meV}$, $c = 34.408$, $m = 8$, $n = 10$ and the lattice parameter $a_0 = 3.92\,\text{Å}$.

As the Sutton–Chen potentials contained a many-body term, they can describe surface effects of metals adequately, and particularly predict an inward relaxation of atoms at the surface of a metal. This is why this potential was chosen in this work for the Pt NW where a large part of atoms are located at the wire surface.

The Sutton–Chen potentials were developed primarily for computer modelling and are analytic and computationally efficient. However, the potentials favour the fcc structure over bcc metals, and the stacking fault energy is practically zero [17]. Another drawback of the potentials is that they neglect the angular bond forces [19] and this was suspected to influence the prediction of the exchange route for surface migration [20]. It was reported in [21] that the melting points of rhodium, silver and iridium are approximately correct but those of platinum and gold are too low; and while trends in most surface properties of fcc metals were reproduced by the potentials, the surface energies tended to be too low and the surface relaxation too high.

Since the Sutton–Chen potentials were parameterised for bulk materials, they work excellently for infinite models and clusters of size greater than 2 nm corresponding to a number of atoms greater than 300 [22]. When used for smaller models, the performance may be affected. For instance, Joswig and Springborg [23] reported that the bond length of an Al diatomic cluster was calculated by the Sutton–Chen potential as 2.09 Å, much below the experimental bond length of 2.47 Å of the diatomic. They used the expression $(mca^k/n)^{1/k}$ for the calculation. Similarly the bond length of a Pt diatomic cluster can be obtained as 2.256 Å, also much lower than the bulk bond length of 2.772 Å. Therefore reliability of the bond lengths for small models obtained by the Sutton–Chen potentials may be a problem. Kaszkur and Mierzwa [24] showed that the SC scheme gave reliable cluster geometry and dynamics for 20-Å clusters. For smaller ensembles the scheme needs to be corrected as probably the square-root-like cohesive term of the potential is inaccurate or the parameter coupling the attractive and repulsive part of the potential (c in the SC scheme) has to be made dependent on the local co-ordination.

3. Simulation method

Using the Sutton–Chen many body potential, the interaction between atoms was truncated at 2.7 a_{nn} where a_{nn} is the nearest-neighbour distance: $a_{\text{nn}} = a_0/2^{1/2} = 2.772\,\text{Å}$. Periodic boundary condition (PBC) was considered only in the axial direction of the NWs to simulate wires with infinite length.

The Newton's equations of MD were integrated using the velocity Verlet algorithm [25] with a timestep $\Delta t = 2\,\text{fs}$. To control temperature in the simulation, the Berendsen thermostat [26] was applied with a characteristic relaxation time of 2.5 ps.

Initial configurations of the Pt NWs were obtained by randomly arranging positions of atoms with a criterion that distance between atoms was not less than 2.3 Å. This distance criterion is a compromise between the feasibility of randomly generating the positions and a reasonably confined volume of the initial configuration. As this distance is much smaller than the lattice nearest-neighbour

distance a_{nn}, a minimisation procedure was first performed by the steepest descendent method (SDM) to relax the initial configurations.

After minimisation, simulated annealing was conducted. At first the NWs were assigned a temperature of 601 K, in that velocities of the atoms were specified with a Maxwell–Boltzmann random distribution. Then the MD simulation was carried out for 200 cycles. In each cycle, the temperature was reduced by 3 K for the first step that followed by 9999 steps involving temperature control. Therefore the simulation time for each cycle was 20 ps and this simulated annealing phase lasted 4 ns. The initial temperature of 601 K was chosen so that the final temperature was approximately 1 K instead of 0 K which should be avoided in the simulation, otherwise temperature control would encounter a numerical problem. When the annealing phase finished, configurations of the NW became stable.

However, force in the NW along the axial direction may not be equal to zero at the end of the above stage. So another MD simulation phase was executed with 50 cycles to achieve a zero-stress state in the NWs. At the first step in each cycle, the residual force in the NW was measured from results of the previous cycle and the length of the NW was adjusted accordingly. This was followed by 9999 relaxation steps with fixed NW length and temperature control. In all cases, the simulation converged to a stable NW length before the completion of 50 cycles.

To assess structural properties of the simulated Pt NWs, we conducted numerical stretching experiments by further MD simulations to measure the Young's modulus of the simulated nanowires. The simulations began from the final configurations which were under approximately zero stress at 1 K. Each simulation has been carried out for a number of cycles with 10,000 time integration steps per cycle. At the first step, a unit strain ($\Delta\varepsilon_z = 0.004$) was applied to the NW following the procedure presented by Finbow *et al.* [16]; (i) the z components of all interatomic vectors r_{ij} were scaled by a factor h_{zz} ($h_{zz} = 1 + \Delta\varepsilon_z$); and (ii) the length of the NW was adjusted with an increment of ΔL_z. The increment $\Delta L_z = L_z(1)\Delta\varepsilon_z$, where $L_z(1)$ is the length of the NW at the final configuration. In this manner, the NW length was allowed to increase linearly with time. The last 2000 steps in each cycle were the product stage. The stress for the cycle was obtained by computing the stress at each step and averaging over the 2000 steps. The stress of the Pt NW along the axial direction was calculated from atomic trajectories, given by [27]:

$$\sigma_z = \frac{1}{N\Omega}\sum_{i>j} f_{ijz} r_{ijz} \tag{3}$$

where N is the number of atoms in the NW, Ω is the atomic volume of platinum and f_{ijz} and r_{ijz} denote z-components of the force vector f_{ij} and the distance vector r_{ij}, respectively, between atom pairs.

In this study we were concerned with only the elastic stretching of the NWs. So the simulations were terminated before plastic-yielding deformations appeared.

4. Results and discussion

We simulated a Pt NW of 169 atoms with an initial length of 25 Å. The final configuration is illustrated in figure 1, which consists of 18 layers with a final length of 24.224 Å. At first glance, the final configuration looks like a filled NW consisting of fcc (1 1 1) layers as reported by Bilalbegovic [2]. By denoting atoms in alternate layers with different greyscales as shown in figure 1, however, we found the axis of the NW is actually along the [1 1 0] direction. Atoms in cross-section were arranged in a pattern as fcc (1 1 0) plane. But there were six columns of atoms, which are indicated in figure 1(b) by surrounding circles, being away from locations where they should be in an ideal (1 1 0) fcc facet. These dislocations could be due to movement of the atoms that were driven by surface energy so that the system can achieve an equilibrium condition at the side boundary.

Another Pt NW of 340 atoms is shown in figure 2. For this NW, the length was initially 23.9 Å and finally became 23.26 Å also including 18 layers. Again the axis of the NW is along the [1 1 0] direction of the fcc lattice. It is interesting to note that the arrangement pattern of the atoms in the cross-section of this NW is different from that of the previous one. There was a symmetry line in

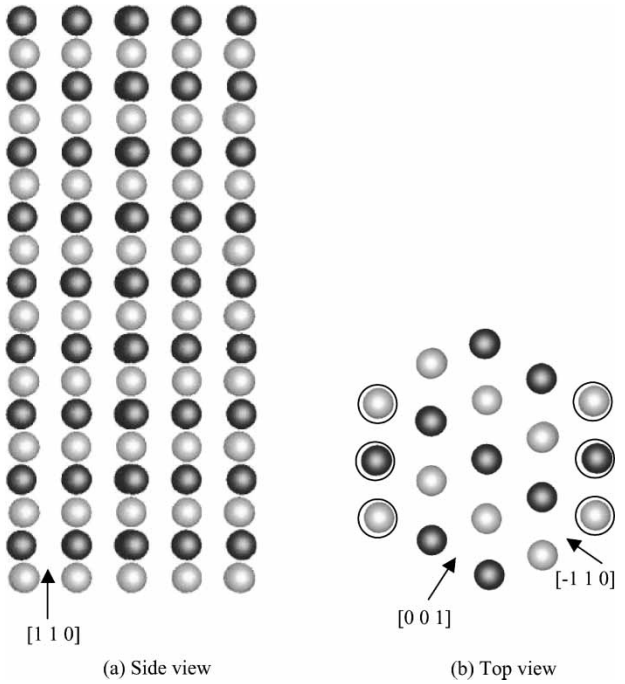

Figure 1. Final configuration at 0 K of the Pt NW with 169 atoms: (a) side view; (b) top view. The length was initially 25 Å and finally became 24.22 Å. The dark- and light-grey colours denote atoms in alternate layers. The NW consisted of 18 layers with fcc (1 1 0) facets. Six columns of atoms were deviating from their ideal locations in cross-section along the fcc [0 0 1] direction.

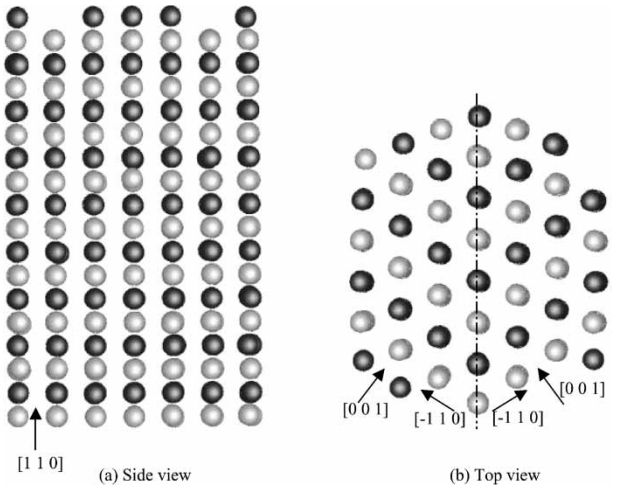

Figure 2. Final configuration at 0 K of the Pt NW with 340 atoms: (a) side view; (b) top view. The length was initially 23.9 Å and finally became 23.26 Å. The NW consisted of 18 layers with fcc (1 1 0) facets. There was a line of symmetry in cross-section; atoms on both sides of the line were arranged in different fcc [0 0 1] directions. The two directions were symmetric with respect to the line.

the cross-section as indicated by the dash-dotted line in figure 2(a). Atoms on both sides of this line were arranged in a pattern along their respective [0 0 1] fcc directions. The two directions are not coincidental but symmetric with respect to the symmetry line. Atoms on the symmetry line were shared by the two groups on both sides.

Shown in figure 3 is the third NW with 770 atoms organised in 24 layers in the final configuration. The length was initially 33.4 Å and finally 32.79 Å, and also extended along the fcc [1 1 0] direction. Similar to the first NW, we observed five columns of atoms deviating from their ideal locations in the fcc (1 1 0) plane. For the other

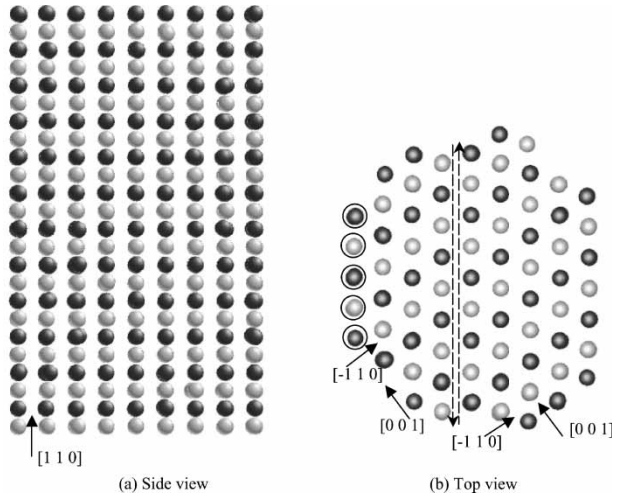

Figure 3. Final configuration at 0 K of the Pt NW with 770 atoms: (a) side view; (b) top view. The length was initially 33.4 Å and finally became 32.79 Å. The NW consisted of 24 layers with fcc (1 1 0) facets. Five columns of atoms deviated from their ideal locations in cross-section. There was a slip line in cross-section; atoms on both sides of the line were arranged in an identical fcc [0 0 1] direction but there was a relative slippage along the line between the two groups of atoms.

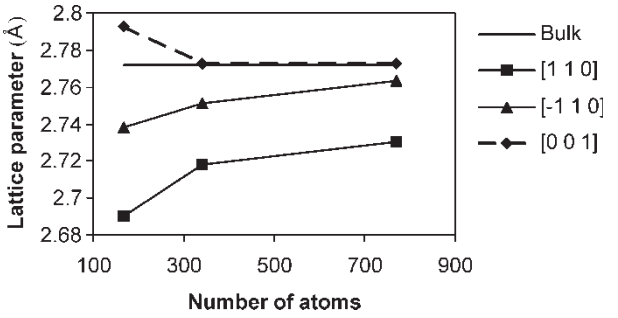

Figure 4. Lattice parameters along three directions versus number of atoms in the simulated platinum nanowires comparing with lattice parameter of platinum bulk material.

atoms, which were all arranged in an identical fcc [0 0 1] direction in cross-section, we detected that they are organised into two groups. There was a relative slippage between the two groups. The slip plane was indicated by a pair of dashed arrows in figure 3(b).

We have measured the lattice parameters of the three NWs in the final configurations and the results are shown in figure 4 in comparison to the bulk nearest-neighbour distance a_{nn}. It can be seen that the calculated data deviate from the bulk value but approach to the later for larger size of NWs. This should be due to the inaccuracy of the Sutton–Chen potentials in computing bond length, as we discussed above. In detail, the average distances between

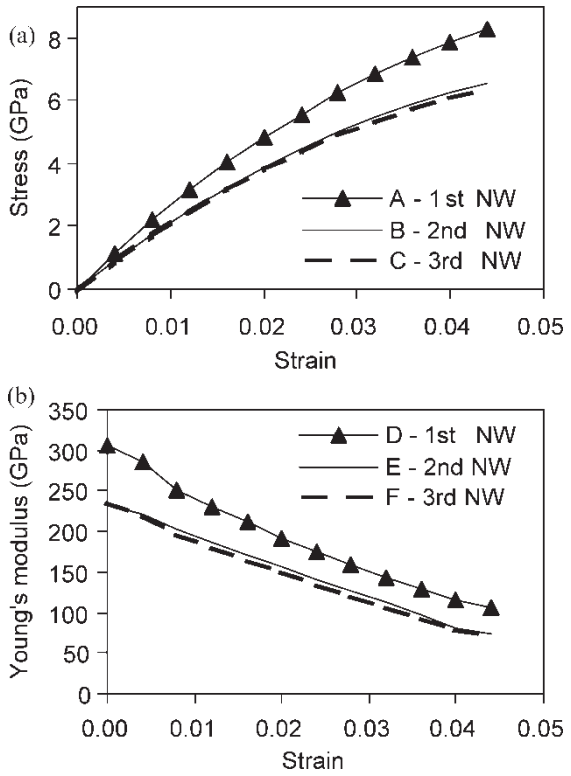

Figure 5. (a) Stress-strain and (b) Young's modulus–strain curves of simulated Pt NWs. Stress values were computed in MD simulations by stretching the three Pt nanowires beginning from their final configuration. Young's modulus was obtained by differentiating the stress-strain curves. Curves A and D are for the NW in figure 1, B and E for the one in figure 2 and C and F for that in figure 3.

the nearest-neighbouring atoms in the three NWs were, respectively, 2.690 Å, 2.718 Å and 2.73 Å in the [1 1 0] direction, 2.738 Å, 2.751 Å and 2.763 Å in the [−1 1 0] direction, and 2.793 Å, 2.773 Å and 2.773 Å in the [0 0 1] direction. We can see that the average nearest-neighbour distances in the [1 1 0] and [−1 1 0] directions in these simulated NWs are shorter than the bulk parameter but increase with an increase in the NW diameters. On the contrary, the average nearest-neighbour distance in the [0 0 1] direction is greater than the bulk parameter but decrease with an increase in the NW diameters.

Stress–strain curves computed from the simulations are plotted in figure 5(a). The deformation of these NWs is non-linear even in the elastic range. By differentiating stress with respect to strain for these curves, we obtained variations of Young's modulus with strain as shown in figure 5(b). It can be seen that the Young's modulus decreased with the stretching of these wires. The thinnest NW (figure 1) had the highest modulus but moduli of the other two NWs were similar. The initial Young's moduli of the wires were 306, 233 and 234 GPa, respectively. As the bulk Young's modulus of platinum is168 GPa, we note that thin Pt NWs are very stiff in comparison to the bulk material.

5. Conclusions

In summary, we used classical MD simulations to study structural formation of Pt NWs with an initial random distribution of atoms. We observed that the final configurations of these wires had a hexagonal solid structure consisting of fcc (1 1 0) layers. The layer structure is different from previously reported simulation results by other investigators. Further, MD simulations were performed to measure mechanical properties by numerical stretching experiments. We found that Young's modulus of these wires was higher than bulk values and the thinnest Pt NW was the stiffest one. The reason causing to form different NW structures would be investigated in the future.

References

[1] Y. Kondo, K. Takayanagi. Synthesis and characterisation of helical multi-shell gold nanowires. *Science*, **289**, 606–608 (2000).

[2] G. Bilalbegovic. Metallic nanowires: multi-shelled or filled? *Comp. Mater. Sci.*, **18**, 333–338 (2000).

[3] G. Bilalbegovic. Multi-shell gold nanowires under compression. *J. Phys. Condens. Mater.*, **13**, 11531 (2001).

[4] G. Bilalbegovic. Structure and stability of finite gold nanowires. *Phys. Rev. B*, **58**, 15412–15415 (1998).

[5] G. Bilalbegovic. Structures and melting in infinite gold nanowires. *Solid State Commun.*, **115**, 73–76 (2000).

[6] J.W. Kang, H.J. Hwang. Molecular dynamics simulation study of the mechanical properties of rectangular Cu nanowires. *J. Korean Phys. Soc.*, **38**, 695–700 (2001).

[7] J.W. Kang, H.J. Hwang. Mechanical deformation study of copper nanowire using atomistic simulation. *Nanotechnology*, **12**, 295–300 (2001).

[8] J.W. Kang, H.J. Hwang. Pentagonal multi-shell Cu nanowires. *J. Phys. Condens. Matter*, **14**, 2629–2636 (2002).

[9] J.W. Kang, H.J. Hwang. An atomistic simulation study of cylindrical ultrathin Cu nanowires. *Mol. Simul.*, **28**, 1021–1030 (2002).

[10] J.W. Kang, H.J. Hwang. Molecular dynamics simulations of ultrathin Cu nanowires. *Comp. Mater. Sci.*, **27**, 305–312 (2003).

[11] A. Hasmy, P.A. Serena, E. Medina. Molecular dynamics simulations for metallic nanosystems. *Mol. Simul.*, **29**, 427–435 (2003).

[12] Y. Oshima, H. Koizumi, K. Mouri, H. Hirayama, K. Takayanagi. Evidence of a single-wall platinum nanotube. *Phys. Rev. B*, **65**, 121401(R)1–121401(R)4 (2002).

[13] T.R. Gao, Z.Y. Chen, Y. Peng, F.S. Li. Fabrication and optical properties of platinum nanowire arrays on anodic aluminium oxide templates. *Chin. Phys.*, **11**, 1307–1312 (2002).

[14] L.B. Kong, M. Lu, M.K. Li, X.Y. Guo, H.L. Li. Morphology of platinum nanowire array electrodeposited within anodic aluminium oxide template characterised by atomic force microscopy. *Chin. Phys. Lett.*, **20**, 763–766 (2003).

[15] V. Rodrigues, D. Ugarte. Metal nanowires: atomic arrangement and electrical transport properties. *Nanotechnology*, **13**, 404–408 (2002).

[16] G.M. Finbow, R.M. Lynden-Bell, I.R. McDonald. Atomistic simulation of the stretching of nanoscale metal wires. *Mol. Phys.*, **92**, 705–714 (1997).

[17] A.P. Sutton, J. Chen. Long-range Finnis-Sinclair potentials. *Phil. Mag. Lett.*, **61**, 139–146 (1990).

[18] M.W. Finnis, J.E. Sinclair. A simple empirical N-body potential for transition metals. *Phil. Mag. Lett.*, **50**, 45–55 (1984).

[19] I. Vilfan, F. Lançon, E. Adam. Lattice vibrations and stability of reconstructed (110) noble metal surfaces. *Surf. Sci.*, **440**, 279–289 (1999).

[20] R.M. Lynden-Bell. Migration of adatoms on the (100) surface of face-centred-cubic metals. *Surf. Sci.*, **259**, 129–138 (1991).

[21] B.D. Todd, R.M. Lynden-Bell. Surface and bulk properties of metals modelled with Sutton–Chen potentials. *Surf. Sci.*, **281**, 191–206 (1993).

[22] Z. Kaszkur. Direct observation of chemisorption induced changes in concentration profile in Pd–Au alloy nanosystems via *in situ* X-ray powder diffraction. *Phys. Chem. Chem. Phys.*, **6**, 193–199 (2004).

[23] J.O. Joswig, M. Springborg. Genetic-algorithms search for global minima of aluminum clusters using a Sutton–Chen potential. *Phy. Rev. B*, **68**, 085408–0854089 (2003).

[24] Z.A. Kaszkur, B. Mierzwa. Segregation in model palladium-cobalt clusters. *Phil. Mag. A*, **77**, 781–800 (1998).

[25] M.P. Allen, D.J. Tildesley. *Computer Simulation of Liquids*, Clarendon Press, Oxford (1987).

[26] H.J.C. Berendsen, J.P.M. Postma, W.F. van Gunsteren, A. DiNola, J.R. Haak. Molecular dynamics with coupling to an external bath. *J. Chem. Phys.*, **81**, 3684–3690 (1984).

[27] M.F. Horstemeyer, M.I. Baskes, S.J. Plimpton. Length scale and time scale effects on the plastic flow of fcc metals. *Acta Mater.*, **49**, 4363–4374 (2001).